Journal of Materials Chemistry C

RSC Publishing

PAPER

View Article Online
View Journal

Cite this: DOI: 10.1039/c3tc31122h

Hierarchically structured, blue-emitting polymer hybrids through surface-initiated nitroxide-mediated polymerization and water templated assembly†

Giuseppe Leone,* Umberto Giovanella, Fabio Bertini, Sajjad Hoseinkhani, William Porzio, Giovanni Ricci, Chiara Botta and Francesco Galeotti*

A facile and robust approach for fabricating structured, blue-emitting polymer hybrids is explored by grafting poly(styrene) incorporating π-conjugated oligo(fluorene) side-chains, to fluoromica silicate layers through surface-initiated nitroxide-mediated polymerization (SI-NMP). It is expected that the polymer intercalation can effectively reduce π-stacking, chain–chain interactions, twists and bends, and interfacial effects, leading to significant difference in the electronic/optoelectronic properties, and improved optical, thermal and chemical stability of the materials. The experimental results indicate that the bottom-up strategy is rational and efficacious. The hybrids exhibit a blue photoluminescence quantum yield (PL-QY) as high as 0.90, even in the solid, which makes the materials appealing for polymer light-emitting devices (PLEDs). The materials also show significantly enhanced thermal, and chemical stabilities with respect to the organic precursors. If processed under specific controlled conditions, the hybrids spontaneously assemble into highly ordered microporous films, where an organization of matter at different length scales is obtained. Since the introduction of surface patterning in the active layer could enhance the extraction of light generated in the device, this hierarchical organization is a promising tool for the further development of optimized hybrid PLEDs.

Received 11th June 2013
Accepted 7th August 2013

DOI: 10.1039/c3tc31122h

www.rsc.org/MaterialsC

1 Introduction

Hierarchical hybrid composites are widely observed in nature, where specific functionalities are often obtained by structuring the matter across a range of length scales. The supramolecular organization of chlorophyll molecules in poly(peptide) cages, involved in photosynthesis, explains, for instance, why plants are such efficient optoelectronic systems. This peculiarity of nature has inspired scientists to design and process organic–inorganic hybrids, in which both phases are intimately combined, optimizing complementary properties and functions (*e.g.*, density, permeability, mechanics).[1] A key example in this context is given by the intercalation of conjugated polymers such as poly(fluorene)s (PFs), poly(aniline), poly(thiophene), poly(*p*-phenylene) in between layered solids, *i.e.*, silicates,[2] V_2O_5 and MoO_3 metal oxide,[3] and chalcogenide compounds MoS_2 and SnS_2,[4] with the aim of enhancing their light emissive properties. In particular, PFs have emerged as semiconducting materials for applications in PLEDs because of the high PL-QY, wide band gaps, and good charge-transport properties.[5] However, PLEDs fabricated from PF-type materials suffer from non-pure emission (green or greenish-blue rather than pure blue) and poor stability against oxygen and moisture. In this respect, the polymer intercalation turns out to be an effective method: (i) to impose constraints on the mesoscopic and molecular structures of the polymer (*i.e.*, reduced π–π stacking, chain–chain interactions, twists and bends, and interfacial effects), (ii) to prevent oxygen and moisture from penetrating into the emissive layer, preserving the emitter against degradation, while retaining a high degree of optical transparency, and (iii) to improve the bulk mechanical properties (*i.e.*, strength, modulus and toughness).[2d,4]

Layered silicates are particularly appealing for fabricating such functional hybrids due to their adsorptive properties, ion-exchange ability and high specific surface area, which permit them to easily tune the interaction between the emitting centers by surface chemistry and a sandwich-type intercalation.[6] The materials can be prepared by two strategies. The first one involves the direct assembly of a pre-formed polymer from the solution method or the exfoliation–adsorption process.[2,4] The second strategy, *i.e.*, bottom-up approach, implies the material's construction using precursors that become organized mainly through chemical processes.[7] In this context, SI-NMP represents a valuable expedient for the fabrication of polymer brushes and hybrid nanoassemblies.[8] An advantage of SI-NMP is that no metal catalysts are required. This obviates the need for additional purification steps and reduces the chance of

CNR Istituto per lo Studio delle Macromolecole (ISMAC), via E. Bassini 15, 20133 Milano, Italy. E-mail: giuseppe.leone@ismac.cnr.it; francesco.galeotti@ismac.cnr.it

† Electronic supplementary information (ESI) available: ^{1}H NMR of St-Fl$_3$. DSC and TGA/DTG curves. Normalized UV-Vis spectra. See DOI: 10.1039/c3tc31122h

introducing impurities, which is advantageous, especially for sensitive applications. A further advantage provided by this approach is that incompatibility between the hydrophilic inorganic component and the hydrophobic polymer is strongly reduced, and hence, the segregation of single-phase microdomains is overcome. In addition, control over the electronic structure and the interlayer geometrical conformation of the polymer can be achieved by a judicious choice of (co)monomers and by tuning the initiator grafting density.[9] As a consequence, not only the primary structure but also the higher-order structures of light-emitting polymers can be tailored to achieve advanced functions. The fabrication of hierarchical structures is a key example in this context, as a way of developing materials with high level of sophistication and miniaturization, which are at the same time robust and adaptable for high value-added applications (*i.e.*, smart membranes and solid support for sensors).[10] Self-assembly is one of the most reliable ways to construct higher-order and even hierarchical structures. The stepwise fabrication of such integrated hybrids with the help of self-organization processes would therefore have the capability of producing patterned film surfaces in a simple and cost-effective manner, thus eliminating the need for external-field and lithography techniques, *i.e.*, top-down strategies. In particular in PLEDs, since most of the light generated in the active layer of a device with conventional architecture remains entrapped as waveguide and substrate modes, the organization into patterned films is functional in introducing a perturbation in the waveguide modes, which may enhance the light outcoupling.[11]

In this work, we describe a two-step method for fabricating blue-emitting poly(styrene) with oligo(fluorene) side-chains/silicate hybrids, in the form of films. The strategy involves the direct addition of the silicate, pre-intercalated by 2,2,6,6-tetramethyl-1-piperidyloxyl (TEMPO) bearing an ammonium functional moiety, to the (co)monomers mixture, *i.e.*, styrene and styrene derivatives *para*-substituted with (oligo)fluorene moieties, followed by SI-NMP. Successively, the polymer hybrids were allowed to self-assemble into microporous films, by applying the breath-figure (BF) templating conditions.[12]

The experimental results indicate that the approach is rational and efficacious: the hybrid composites exhibit high solution-processability, improved thermal stability, and the blue PL-QY as high as 0.90, even in the solid state, which makes the materials appealing for PLEDs. Moreover, the adjustment of overall hydrophilicity of the material, through a proper balancing of the amounts of the components, led to hierarchically structured hybrids in the form of patterned films organized at two different length scales, *i.e.*, intercalated polymer chains and micrometric periodic structures, which offer significant promise as a platform for the further development of non-planar PLEDs and other technological applications.

2 Experimental

2.1 Materials

Manipulations of air- and/or moisture-sensitive materials were carried out under an inert atmosphere using a dual vacuum/nitrogen line and standard Schlenk techniques. Fluoromica silicate, *i.e.*, Somasif ME100 (SME) (CO-OP Chemicals), was dried at 130 °C under reduced pressure (10^{-3} bar) for two weeks and then it was stored under nitrogen. Rhodamine 6G (R6G, Acros Organics, dye content 99%), 4-acetamido-2,2,6,6-tetramethylpiperidine 1-oxyl radical (Sigma-Aldrich, ≥98% pure), $Pd(PPh_3)_4$ (Sigma-Aldrich, ≥99% pure), 9,9-dioctylfluorene-2,7-bis(trimethyleneborate) (Sigma-Aldrich, ≥97% pure), 2,7-dibromo-9,9-dioctylfluorene (Sigma-Aldrich, ≥96% pure), and 4-vinylphenylboronic acid (Sigma-Aldrich, ≥98% pure) were used as received. 2-Bromo-9,9-dioctylfluorene was synthesized according to a literature procedure.[13] Ethyl alcohol (Carlo Erba, 96% pure) and *ortho*-dichlorobenzene (*o*-DCB) (Sigma-Aldrich, anhydrous grade) were degassed under vacuum then by bubbling nitrogen, kept over molecular sieves and used without any further purification. Diethyl ether (Fluka, ≥99.5% pure) and THF (Sigma-Aldrich, ≥99.0% pure) were refluxed over Na/K benzophenone for *ca.* 8 h, then distilled and stored over molecular sieves under nitrogen. Carbon disulfide, methanol, hexane, and toluene (Sigma-Aldrich) were used without further purification. Styrene (Sigma-Aldrich, 99% pure) was refluxed for 4 h over calcium hydride, then distilled trap-to-trap and stored under nitrogen. Distilled deionized water was used for all cation-exchange experiments.

2.2 Synthesis of the TEMPO-like nitroxide cation

4-Acetamido-2,2,6,6-tetramethylpiperidine 1-oxyl radical (0.5 g, 2.92 mmol) was placed into a 50 mL three-neck round bottomed flask charged with diethyl ether (25 mL), allowed to stir for 1 h at 24 °C and then washed with HCl (aq., 1 M, 3 × 5 mL). The aqueous layers were combined and the solvent was removed under vacuum for several days. The product was obtained as red powder.[14] FTIR (nujol): 2926 (br, s), 2365 (m), 2339 (m), 1622 (m), 1611 (m), 1522 (m), 1479 (m), 1391 (s), 1352 (w), 1243 (m), 1223 (w), 1178 (w), 1095 (m), 1018 (w), 953 (w), 886 (w), 744 (m) cm^{-1}.

2.3 (Co)intercalation of R6G and the TEMPO-like cation

G7 was synthesized according to the procedure previously reported.[14] Typically, to a 250 mL three-neck round bottomed flask, equipped with a stirring bar, were added SME (402 mg) and water (150 mL). The mixture was stirred for 4 days at room temperature. A solution of the TEMPO salt (52.4 mg, 0.34 mmol) in ethanol is prepared. A solution of R6G (72.7 mg, 0.16 mmol) in ethanol is prepared. The aimed loading for the sample G7 is 70% and 34% of the total SME cation exchange capacity (CEC) for TEMPO and R6G cations, respectively. Both the R6G and TEMPO-like cation solutions were added to the SME suspension in water. The cation-exchange reaction proceeds for an additional 48 h at room temperature. To collect the loaded SME, the suspension was filtered and washed with a water–ethanol mixture (1 : 1). Once the solvent was removed under reduced pressure, the product was extracted with ethanol through a Soxhlet method for 8 h. The residual fraction was dried in a vacuum and then ground in the agate mortar. FTIR (KBr): (νC–H, 2852 cm^{-1}; δC–H, 1343 cm^{-1}), (νN–O, 1391 cm^{-1}), (νC–N, 1261 cm^{-1}), (νN–H, 1519 cm^{-1}), (νC–H, 1320 cm^{-1}), 1611,

1529, and 1501 cm^{-1} associated with in-plane vibration of the R6G xanthene ring, and νC=O, 1721 cm^{-1}. The contents of TEMPO and R6G were 12.0 and 4.1 wt%, respectively.[14]

2.4 9,9-Dioctyl-2-(9,9-dioctyl-2-(9,9-dioctyl-2-(4-vinylphenyl)-9*H*-fluoren-7-yl)-9*H*-fluoren-7-yl)-9*H*-fluorene (St-Fl_3)

It was synthesized through a stepwise Suzuki coupling approach, as depicted in Scheme S1.† A mixture of 2-bromo-9,9-dioctylfluorene (500 mg, 1.07 mmol), 9,9-dioctylfluorene-2,7-bis-(trimethyleneborate) (1.492 g, 2.67 mmol), K_2CO_3 (2.0 M aqueous solution, 4.0 mL), $Pd(PPh_3)_4$ (61 mg, 0.05 mmol) and THF (9 mL) were placed in a Schlenk flask and stirred at 55 °C for 48 h. After cooling to room temperature, the reaction mixture was poured into a large excess of petroleum ether. The organic layer separated was washed with brine and dried over anhydrous Na_2SO_4. After filtration and evaporation of the solvent, the crude product was purified by column chromatography on silica gel with hexane to afford the borolane terminated dimer as white crystals (Fl_2, 370 mg, 40%). ^{1}H NMR (600 MHz, $CDCl_3$): (δ, ppm) 7.36–7.28 (m, 13H, Ar), 4.21 (t, 4H, –OCH_2–), 2.02 (m, 8H, $C(CH_2C_7H_{15})_2$), 1.53 (m, 2H, –OCH_2CH_2–), 1.17–1.06 and 0.79–0.67 (m, 60H, $C(CH_2C_7H_{15})_2$). In the following step, Fl_2 (325 mg, 0.38 mmol) and 2,7-dibromo-9,9-dioctylfluorene (330 mg, 0.565 mmol) were allowed to react as mentioned in the previous step. After 20 h, 4-vinylphenylboronic acid (118 mg, 0.80 mmol) was added to the reaction mixture and allowed to react at 45 °C for another 96 h. The same workup and column separation as that mentioned above gave St-Fl_3 as a light yellow semisolid (280 mg, 58%). ^{1}H NMR (600 MHz, $CDCl_3$): (δ, ppm) 7.76–7.50 (m, 23H, Ar), 6.78 (m, 1H, –CH=), 5.79 (m, 1H, =CH), 5.27 (m, 1H, =CH), 2.02 (m, 12H, $C(CH_2C_7H_{15})_2$), 1.24–1.04 and 0.79–0.70 (m, 90H, $C(CH_2C_7H_{15})_2$). Anal. calcd for $C_{95}H_{128}$: C, 89.84; H, 10.16%. Found: C, 89.67; H, 10.22%.

2.5 SI-NM(co)polymerization of styrene with St-Fl_3

The polymerizations were carried out in a 25 mL round bottomed Schlenk flask, which had been dried on the high vacuum line by heating at 80 °C, and equipped with a magnetic stirring bar. The reactor vessel was charged with G7, *o*-DCB, styrene, and St-Fl_3 in that order. The reaction mixture was degassed by nitrogen bubbling for 20 min. The polymerization was carried out at 125 °C for 17 h. When the system was cooled to room temperature, polymerization was stopped by addition of methanol (20-fold excess). The precipitated polymer was collected by filtration, repeatedly washed with fresh methanol and then dried in a vacuum to constant weight. The product was then extracted with methanol through a Soxhlet method for 10 h to completely remove the unreacted St-Fl_3 comonomer. The residual fraction was dried in a vacuum. The amount of G7, styrene, and St-Fl_3 in the polymer hybrids was determined from thermogravimetric analysis (TGA) data, according to Smitha *et al.*[15] TGA data useful for evaluating the composition of the polymer hybrid (PF1–3) are reported in Table S1.†

2.6 Films preparation

Films for optical characterization were obtained by casting or spin-coating 17 mg mL^{-1} toluene solution of the compound on a glass substrate. Honeycomb structured films were obtained by casting 150 μL of a carbon disulfide solution of the polymer hybrid on a 1.5 × 1.5 cm^2 glass cover slip under a flow of moist air (60% R.H. at 25 °C), obtained by flowing air at 2 L min^{-1} through a two-necked flask filled with water, at ambient temperature. Polymer concentration was varied from 5 to 10 mg mL^{-1} in order to set the optimal conditions for BF formation.

2.7 Characterization techniques

FTIR spectra were recorded by a Bruker IFS 48 spectrometer. Size exclusion chromatography (SEC) measurements were carried out on a Waters SECV2000 system equipped with two PLGel Mixed C columns, a 2414 RI detector and a 490 UV diode-array detector. THF was used as solvent and poly(styrene) with molar masses ranging from 162 to 3.28 × 10^6 g mol^{-1} were used as standards. TGA was performed on a Perkin-Elmer TGA-7 instrument under a nitrogen flow rate of 35 mL min^{-1}. Before performing the TGA run, the sample (2–3 mg) was held at 100 °C for 1 h; the scan was carried out from 100 to 750 °C at a heating rate of 10 °C min^{-1}. The residue of the TGA run was oxidized at 750 °C for 10 min under an air atmosphere (35 mL min^{-1}). Differential scanning calorimetry (DSC) measurements were carried out on a Perkin-Elmer Pyris 1 instrument. The sample, about 5 mg, was placed in a sealed aluminum pan and the measurements were carried out from 40 to 200 °C under a nitrogen atmosphere using heating and cooling rates of 20 °C min^{-1}. X-ray diffraction (XRD) data were obtained at 25 °C using an Anton&Parr Camera under nitrogen flux and a Siemens D-500 diffractometer (Cu K_α radiation, λ = 0.154 nm). The operating voltage and current were 40 kV and 40 mA, respectively. Data were collected from 3° to 33° 2θ at 0.05° 2θ intervals. UV-Visible absorption measurements were carried out *via* PerkinElmer Lambda900. The continuous wave PL spectra were recorded by a liquid nitrogen cooled charge-coupled device combined with a monochromator (Spex 270M), and excited using a monochromated xenon lamp. The spectra were corrected for the instrument's response. PL-QYs of the films have been measured with a home-made integrating sphere.[16] Fluorescence microscopy images were obtained by using a Nikon Eclipse TE2000-U inverted confocal microscope. SEM images were recorded using the Zeiss Leo 982 apparatus at 3 kV tension.

3 Results and discussion

3.1 Synthesis and characterization

Somasif (SME), described by the structural formula $Na_n[Si_{8-n}Al_n]Mg_6O_{20}F_4$, where n represents the unit cell charge, is a semi-synthetic crystalline fluoromica with an aspect-ratio of about 6000, an average charge unit density of 0.77 nm^2, and a CEC of 120 mequiv. 100 g^{-1}.[17] To apply the SI-NMP technique to SME, firstly, we synthesized a TEMPO alkoxyamine bearing an ammonium functional moiety for anchoring to the layer surface by sodium-cation exchange. SME was then organo-modified by (co)intercalation of the TEMPO cation (70% *vs.* CEC) and R6G (34% *vs.* CEC) (sample G7), as we recently reported.[14] R6G ensured the increase of polar functionality of the material,

which was fundamental to form a stable interface with water droplets during BF formation, and allowed us to tag the SME tactoids, thus following the dispersion of the inorganic counterpart in the polymer matrix (see Section 3.3). Subsequently, the macromolecular chains were ionically grafted to the SME layers through the radical copolymerization of styrene with styrene *para*-substituted with the π-conjugated tri(9,9-dioctylfluorene) fragment (St-Fl_3), forming confined extended monolayer poly(St-*co*-St-Fl_3) stripes (Scheme 1). The polymerization experiments were carried out in a round bottomed Schlenk flask, charged with G7, *o*-DCB, styrene and St-Fl_3. Different feedstock comonomers composition ([St]/[St-Fl_3] from 133 : 1 to 9700 : 1) and inorganic/organic ratios were investigated (Table 1). Solvent polymerization was preferred to bulk because we wanted to maintain a high dispersion of the inorganic particles in the reaction medium; *o*-DCB is chosen to facilitate the diffusion of the highly hindered oligo(fluorene) comonomer within the SME layers as a result of the electron withdrawing effect of the benzene ring.

Poly(St-*co*-St-Fl_3) hybrids (PF1–PF3, Table 1) were obtained in high yield, somewhat independent for the initial comonomer mole ratio from 2600 : 1 to 9700 : 1, and then decreased for a St/St-Fl_3 ratio of 133 : 1. Increasing the charged St-Fl_3, the comonomer incorporation in the copolymer raised. Specifically, at a St-Fl_3 feed content as low as 5.62×10^{-4} and 1.36×10^{-3} M (PF1 and PF2, respectively) the St-Fl_3 incorporation does not exceed 1 wt%. St-Fl_3 incorporation as high as 16.7 wt% was reached increasing the St-Fl_3 feed concentration up to 2.19×10^{-2} M (run PF3). SEC analysis yielded a molecular weight of 6.7×10^4 g mol^{-1} for PF3 and *ca.* 19×10^4 g mol^{-1} for PF1 and PF2, suggesting a certain extent of chain transfer reactions over the increase of the charged oligo(fluorene) monomer. In contrast to what one might expect for a controlled SI-NMP, broader than expected molecular weight distribution ($M_w/M_n \approx 2.4$) may be due to trace interlayer water impurities and inadequate kinetic control. Indeed, the polymerizations were carried out in the absence of the free TEMPO agent, while it is well known how the addition of the latter creates an overall concentration of nitroxide in the reaction mixture which controls the polymer chain growth, affording a living polymerization.[8,18] The random copolymers are amorphous by DSC with a narrow range of glass transition temperature values (T_g, 85–87 °C, Fig. S1†). In addition, the synthesized polymer hybrids were thermally stable over 430 °C (T_{deg}, Table S1 and Fig. S2†), which makes them appealing for practical applications.

Table 1 SI-NM (co)polymerization of styrene with St-Fl_3[a]

Run	St/St-Fl_3 (mole ratio)	Yield (g)	G7[b] (wt%)	St[b] (wt%)	St-Fl_3[b] (wt%)	M_w[c] [$\times 10^{-4}$] (g mol^{-1})
PF1	9700	1.25	0.3	99.1	0.6	19.7
PF2	2600	1.15	0.7	98.1	1.2	18.7
PF3	133	0.88	6.6	76.7	16.7	6.7

[a] Polymerization conditions G7, 13 mg (PF3: G7, 65 mg); St, 2.74 g; temperature, 125 °C; time, 17 h and total volume, 10 mL. [b] G7, St and St-Fl_3 contents in the polymer hybrids were determined by TGA. [c] M_w, molecular weight determined by SEC.

We examined the extent of intercalation that takes place as a result of the growth of the macromolecular chains within the SME layers by XRD, determining the (001) basal spacing between the fluoromica platelets, and hence, the calculation of the clearance space between the inorganic layers, namely *d*(free), after the subtraction of the layer thickness.

In Fig. 1, the XRD patterns of the polymer hybrids are shown, together with those of dehydrated SME and G7 precursors. The XRD pattern of SME shows only one diffraction peak at 9.40° 2θ, corresponding to the interlayer spacing of 0.94 nm of sodium exchangeable cation layers.[19] A shift of the (001) diffraction peak toward low angle, and thus an increase of the layer periodicity, was registered for G7, thus providing evidence for the intercalation of organic moieties.[14] Basically, G7 shows almost two diffraction peaks, partially overlapped. By applying peak profile analysis through a pseudo-Voigt function, we found that the broad single peak can be deconvoluted and quantified to fit peaks at 4.65° and 5.85° 2θ, corresponding to the interlayer spacing of 1.90 [*d*(free) = 0.94 nm] and 1.53 nm [*d*(free) 0.57 nm], respectively.

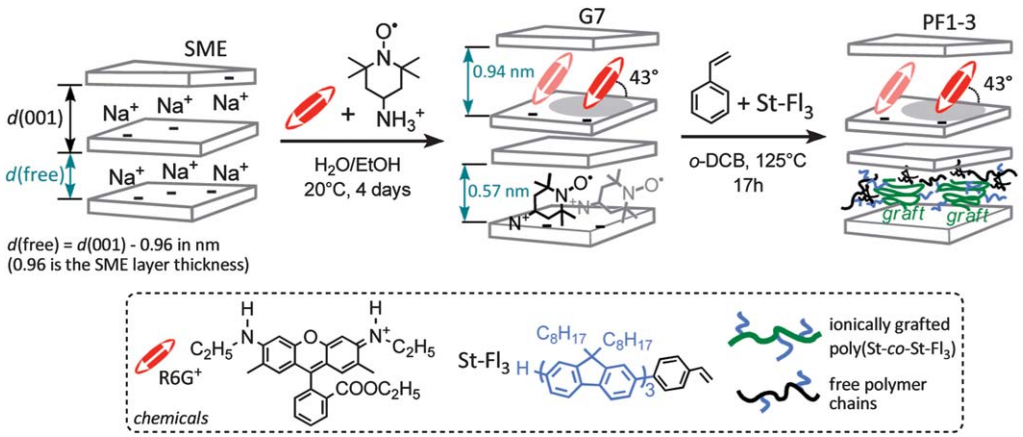

Scheme 1 Schematic and simplified illustration of the polymer hybrids (PF1–3) synthesis.

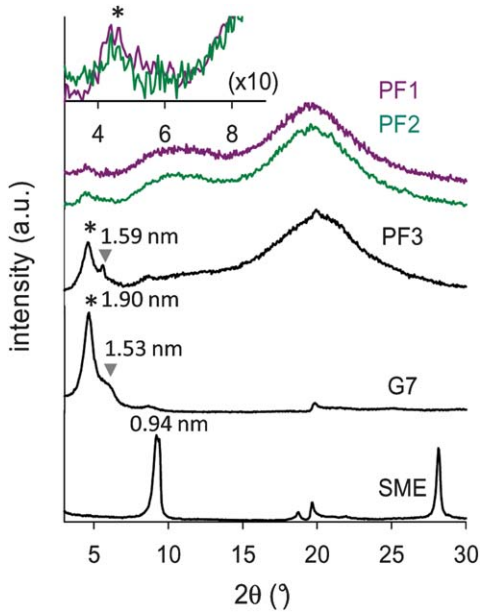

Fig. 1 XRD spectra of (from the bottom to the top) native dehydrated SME, NT/R6G-(G7) intercalated SME, and bulk poly(St-*co*-St-Fl_3) hybrids (PF1–3). The profiles were properly scaled to ease the reading.

The competitive (co)intercalation of R6G and TEMPO-like cations led to mixed-layer structures, in which mainly two kinds of unit layers are arranged along the *c*-axis direction, as schematically shown in Scheme 1. We found that R6G and TEMPO-like cations were intercalated in separate interlayer spacing: the stratification of the (co)intercalated molecules, that is, the segregation of them, was likely due to the fact that the two cations organize within the inorganic layers in distinct arrangements, the TEMPO molecule being small enough to fit well into a single unit charge in a flat monolayer arrangement, and R6G folded up to 43° with respect to the SME layer surface.[14] This phenomenon has been fully described in our previous work,[14] and will be only briefly outlined here. Taking into account the SME layer charge density and the TEMPO molecule size (the thickness is *ca.* 0.4 nm and its long molecular axis *ca.* 0.6 nm), a flat monolayer disposition is consistent with the calculated *d*(free) of 0.57 nm; in such an arrangement there is a reliable match between the area required by an intercalated molecule (0.26 nm^2) and that available (0.77 nm^2). On the other hand, a larger increase of the interlayer space was registered for the R6G intercalated layers. This layers spacing can be explained if a tilted distribution of the R6G long-molecular axis with respect to the SME layer surface, is considered. Taking into account the R6G molecular dimensions (1.38 × 1.15 × 0.9 nm, Scheme 1) and that the *d*(free) is given by the dye long-molecular axis multiplied by the sin of the angle (α) formed between this axis and the surface plane, α was determined by means of $\sin\alpha = d(\text{free})/1.38$ in nm, to be 43°. Such a perpendicular orientation of the dyes, usually observed for high dye loading, is adopted to reduce the inter-electronic π-system dye–dye interactions.[20]

After the polymerization, the resulting PF3 hybrid clearly exhibited two distinct diffraction peaks having maxima at 4.65° and 5.60° 2θ, corresponding to the interlayer spacing of 1.90 and 1.59 nm, respectively. Basically, the former, marked with an asterisk, stems from the layers with R6G exchangeable cations, the *d*(free) being close to 0.94 nm as for the most intense peak of the G7 precursor, indicating that R6G–SME stacks are still present without the intercalated polymer. The second one at 5.60° 2θ, that stems from the intercalated TEMPO-like cations, was shifted to lower 2θ with respect to the peak of the starting G7. Specifically, the height spacing was 0.06 nm larger than that of G7, meaning that only a slight expansion occurred over the TEMPO-mediated polymer chains growth. By subtracting the thickness of SME lamellae from the (001) basal spacing, the maximum thickness of the polymer brushes was calculated to be 0.63 nm [*d*(free) = 1.59 − 0.96 in nm], meaning that the grafted polymer chains adopted an almost extended planar conformation rather than a coiled or a fully extended brush one. This result is in agreement with that obtained for poly(aniline) and poly(9,9-dioctylfluorene) intercalated within layered MoS_2 and SnS_2 chalcogenides, and for poly[2-methoxy-5-(2′-ethylhexyloxy)-1,4-phenylenevinylene] in between layered silicates.[2,4] Even more, the polymer monolayer with flat conformation is consistent with the fact that the SME interlayer spacing did not increase with the polymer molecular weight. Indeed, a similar trend was inferred by XRD for PF1 and PF2 which have a molecular weight three times greater than PF3, although in the first two samples the layer stacking was hardly to be detected likely due to the low inorganic content.

In addition, in the case of PF3, the tightness of the reflection indicates that the layers have restacked to form plates about 25 layers thick (extracted from the full width at half maximum).

3.2 Optical properties

The polymer intercalation with immobilization of pendant St-Fl_3 oligo(fluorene)s in the restricted geometries prevents their aggregation and leads to a planarization of adjacent oligo(fluorene) moieties, causing the extension of the oligomers conjugation length,[2d,4,21] hence affecting the optical properties. Indeed, a bathochromic shift of PL spectra was reported for oligo(fluorene)s with fluorenes linearly fused in a ladder-type conformation together with the appearance of better resolved vibronic features.[22] The UV-Vis absorption and PL properties of the polymer hybrid films are summarized in Table 2 together with those of the St-Fl_3 film and solution.

The absorption spectra of PF1, PF2 and PF3 films and St-Fl_3 solution exhibited a maximum at about 364 nm related to π → π* transition of the St-Fl_3 comonomer, that is red-shifted by about 10–15 nm with respect to tri(9,9-dioctylfluorene)[23] due to

Table 2 Optical properties of polymer hybrid films

Sample	λ_{max}^{abs}	λ_{max}^{PL}	PL-QY
St-Fl_3	366, 364[a]	434, 410[a]	0.62, 0.81[a]
PF1	364	405	0.71
PF2	364	412	0.82
PF3	364	427	0.90

[a] Toluene solution. The PL-QY values are estimated to be ±0.07.

the presence of an additional phenyl ring that extends the conjugation length (Fig. S3†). The fluorescence spectra of PF1 and PF2 showed maxima at 405 and 412 nm, respectively, similar to neat St-Fl$_3$ in solution, while the PF3 emission spectrum was red-shifted with the main peak at 427 nm (Fig. 2). Vibronic side bands typical of fluorene based-oligomers were evident in the PL spectra of the films, better resolved than in the absorption spectra and sharper as the content of St-Fl$_3$ increases (Table 1).

The strong emission efficiency (PL-QY = 0.7–0.8) recorded for St-Fl$_3$ and the hybrid materials PF1–3 in solution was only slightly lower than that of pristine tri(9,9-dioctylfluorene) reported in the literature.[22,24] More interestingly, this high PL efficiency was not reduced in the solid-state, as it occurs for the neat St-Fl$_3$ (Table 2) as well as for other fluorene-based systems, but is retained, and even enhanced, for the polymer hybrid films. In fact, an exceptionally efficient blue-emitting film, with a PL-QY value of about 0.9, can be easily achieved by spin-coating PF3 from toluene solution.

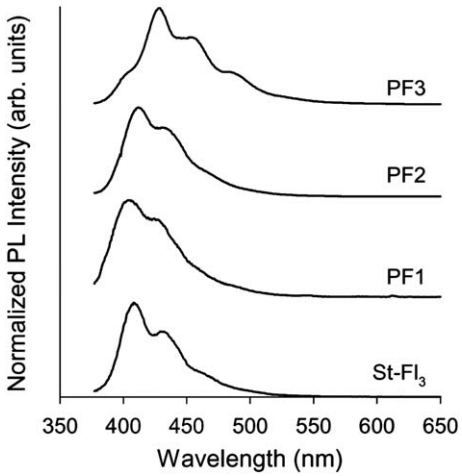

Fig. 2 PL spectra of St-Fl$_3$ solution and the PF1–3 film excited at 370 nm.

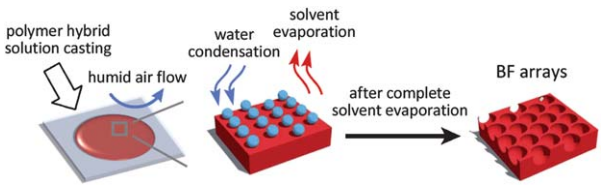

Scheme 2 Schematic step-by-step of the BF fabrication technique.

The high dilution of the non-intercalated St-Fl$_3$ side-chains along the poly(styrene) backbone in PF1 and PF2 films led to optical properties typical of St-Fl$_3$ oligomers in solution (see Table 2). The higher concentration of the oligo(fluorene) side-chains and the fluoromica counterpart in PF3 (Table 1), allows for an efficient energy transfer from the higher energy non-intercalated oligo(fluorene)s to the more planar intercalated ones, leaving only a weak high energy band (around 410 nm) in the PL spectrum of the PF3 film (Fig. 2). As a result, PF3 films showed an enhanced PL-QY due to the emission from highly stable and planar oligo(fluorene) polymer side-chains intercalated within the fluoromica layers.[22a] This superior optical performance in the solid-state as compared to other efficient fluorene derivative emitters[25] suggests the application of PF3 as the electroluminescent layer in a PLED.

3.3 Breath figures formation

To go one step further towards a hierarchically structured material, the polymer hybrids were dissolved in carbon disulfide and allowed to self-assemble into microporous films, by applying the BF templating conditions (Scheme 2). This technique in fact allows for the realization of microporous films with cavities arranged in a packed hexagonal fashion. The phenomenon has already been fully described, and will be only briefly outlined here.[26]

BF formation is driven by the condensation of water droplets on the surface of a polymer solution, cast in a humid atmosphere.

During solvent evaporation the water droplets, stabilized by the polymer, arrange themselves, forming a template for the honeycomb film. When the process is complete, a honeycomb-like imprint of the droplets is left on the polymer film surface. The formation of micropores was observed for all the materials under study (Fig. 3). The presence of both St-Fl$_3$ comonomer and R6G, allowed us to extensively use the fluorescence microscopy to characterize the films obtained.[27] In fact, the blue

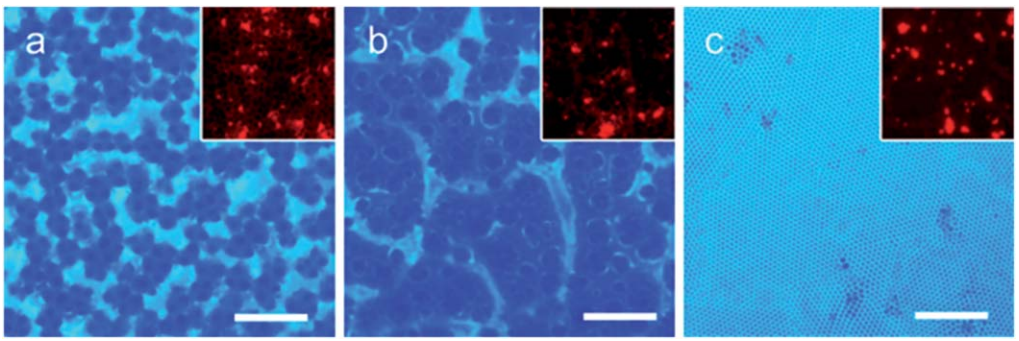

Fig. 3 Fluorescence microscopy images of honeycomb films prepared with different polymer hybrid materials: PF1 (a), PF2 (b) and PF3 (c). Pictures obtained by UV excitation. Insets: reduced views of the same areas by green excitation. Scale bars: 30 μm.

emission of St-Fl_3 highlights the morphology of the polymer film, while the red emission of R6G is useful for simultaneously localize the distribution of the R6G-doped SME stacks (Fig. 3 insets).

Films prepared with PF1 and PF2 both revealed a non-homogeneous and randomly distributed porous morphology. Areas with micrometric pores (1–6 μm) arranged in a more packed way (Fig. 3a and b) and with giant (20–50 μm) irregular cavities were visible within the same film (images not shown).

The modification of the operational conditions, including polymer concentration and the evaporation rate, did not lead to any improvement of the quality of porous films. In contrast, and intriguingly enough, highly ordered honeycomb films were obtained with PF3 (Fig. 3c). Films prepared with this specific polymer hybrid material showed in fact extremely regular cavities having an external diameter of 1.5 μm and a center-to-center distance of 2.3 μm (Fig. 4a and b). The hexagonal arrangement of cavities is homogeneous on the whole film, and the ordered areas without defects, except for the local discontinuities due to the presence of SME tactoids, are as wide as 1 mm^2 (Fig. 4c).

To a closer view (Fig. 4d and e), it is possible to notice that these big aggregates, that exceed the thickness of the film, are coated by a thin layer of polymer, and that this layer is patterned as well. BFs on particles and small objects have been previously observed by using elastomeric core cross-linked star polymers with low T_g,[28] since the soft-flowing nature of these materials allows the honeycomb to contour to non-flat surfaces. Surprisingly, in our case, we achieved a conformal coating of the R6G–SME particles by the patterned film using a poly(St-*co*-St-Fl_3) linear polymer, hence a poorly elastic material. This can be interpreted as further evidence that the inorganic nanoparticles are wrapped by the polymer, as we previously observed by AFM in similar composite materials.[29]

In Fig. 4f, the simultaneous emission of the St-Fl_3 pendants (green matrix) and the R6G (red spots) intercalated within the SME layers is evidenced by fluorescence microscopy with blue excitation light. The green colour of the honeycomb film is due to the filter used, which cuts the blue part of the St-Fl_3 emission band. Once again, the image attests the presence of different levels of organization in the same material: nano-confined St-Fl_3 and R6G in between the SME lamellae and the micro-structured film. This multilevel organization is certainly appealing for an optimization of polymer hybrid-based LEDs. Indeed, the introduction of surface patterning in the active layer could enhance the extraction of light generated in the device.[5]

The reason why PF3 turned out to be so effective in producing honeycomb structures is yet to be clarified. Previously, two different studies have reported on BF films with polymer/silicate hybrid systems, but those films were well far away from the degree of order reached here.[30]

An all polymeric material containing both styrene and oligo(fluorene) moieties, but with a star-polymer nature, was reported to give BF arrays.[31] However, star polymers are known to be particularly suitable for BFs, in fact they were actually observed for the first time with this class of materials.[32] Herein, we have a linear copolymer surrounding nano/micrometric SME particles. We did not observe any regular BF arrays by using pure poly(styrene) or pure St-Fl_3 solutions, which suggests that the presence of fluoromica plays a role in the stabilization of water droplets.[30a] On the other hand, PF1 and PF2, which contain all the components of PF3, but in different ratios, produced only disordered BFs. We can therefore infer that in PF3, apparently, the ratio between SME, R6G and St-Fl_3 amounts are optimized so as to achieve maximal stabilization of water droplets during their formation and arrangement on the solution surface; hence, ordered patterns are obtained.

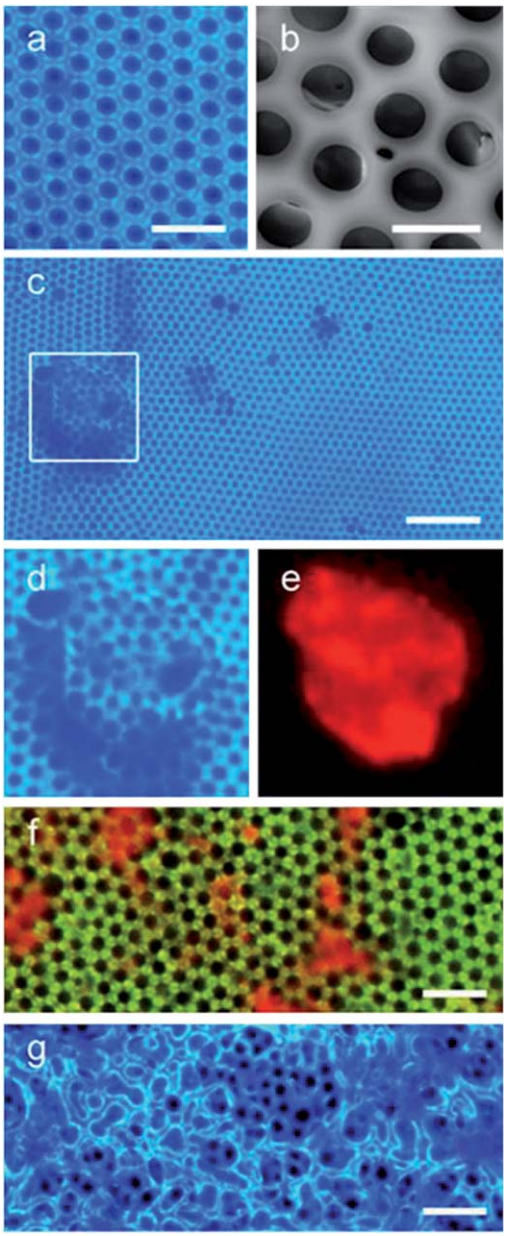

Fig. 4 Microscopy images of PF3 honeycomb films. (a) Close view by fluorescence microscopy (UV excitation, scale bar 4 μm). (b) SEM micrograph (scale bar 2 μm). (c) Wider fluorescence view showing long-range order (scale bar 15 μm). (d) Zoomed detail of the area of (c) in the white square. (e) Same view by green excitation. (f) Fluorescence image by blue excitation (scale bar 5 μm). (g) Fluorescence image of the bottom of the film by UV excitation (scale bar 5 μm).

Fig. 4g shows the fluorescence microscope image of a PF3 patterned film viewed from its bottom face, *i.e.* through the glass cover slip used as the substrate. Remarkably, underneath the regularly arranged micrometric network, a second level of interconnected and disordered voids is visible. Such a foam-like structure suggests that these films are, at least partially, opened at the bottom. This observation, quite uncommon for BFs, opens the way to the possible application of these films as multifunctional membranes.

4 Conclusions

In summary, we have demonstrated a convenient strategy to fabricate hybrid materials comprising a blue-emitting polymer grafted to the fluoromica interlayers surface. The hybrids have been fabricated through a simple, controllable, SI-NMP synthesis. In this way, an intimate mixing of the 'soft' polymer with the 'hard' inorganic component has been promoted, thus preventing nanoparticle aggregation, and making the materials easy to process by solution. Hence, uniform thin-films have been fabricated by spin-coating, showing remarkably high PL efficiency (PL-QY $\approx$ 0.90), which makes the materials appealing for PLEDs. Notably, under optimized conditions, the hybrids spontaneously assemble into highly ordered microporous films, where an organization of the matter at different length scales is obtained. The hierarchically structured hybrids, besides having a good potential in optoelectronics, may be valuable for novel technological applications.

Acknowledgements

The authors thank Mr A. Giacometti Schieroni for SEC characterization and Dr A. Boglia for technical assistance.

Notes and references

1 (*a*) C. Sanchez, H. Arribart and M. M. Giraud-Guille, *Nat. Mater.*, 2005, **4**, 277; (*b*) B. Descalzo, R. Martínez-Máñez, F. Sancenón, K. Hoffmann and K. Rurack, *Angew. Chem., Int. Ed.*, 2006, **45**, 5924; (*c*) D. Yan, J. Lu, W. Mei, D. G. Evans and X. Duan, *J. Mater. Chem.*, 2011, **21**, 13128; (*d*) C. Sanchez, B. Lebeau, F. Chaput and J.-P. Boilot, *Adv. Mater.*, 2003, **15**, 1969; (*e*) C. Sanchez, B. Julián, P. Belleville and M. Popall, *J. Mater. Chem.*, 2005, **15**, 3559.

2 (*a*) T.-W. Lee, O. O. Park, J. Yoon and J. J. Kim, *Adv. Mater.*, 2001, **13**, 211; (*b*) J. H. Park, Y. T. Lim, O. O. Park, J. K. Kim, J.-W. Yu and Y. C. Kim, *Adv. Funct. Mater.*, 2004, **14**, 377; (*c*) C. Chakraborty, K. Dana and S. Malik, *J. Colloid Interface Sci.*, 2012, **368**, 172; (*d*) C. Chakraborty, P. K. Sukul, K. Dana and S. Malik, *Ind. Eng. Chem. Res.*, 2013, **52**, 6722.

3 (*a*) C.-G. Wu, D. C. DeGroot, H. O. Marcy, J. L. Schindler, C. R. Kannewurf, Y.-J. Liu, W. Hirpo and M. G. Kanatzidis, *Chem. Mater.*, 1996, **8**, 1992; (*b*) R. Bissessur, D. C. DeGroot, M. G. Kanatzidis, J. L. Schindler and C. R. Kannewurf, *J. Chem. Soc., Chem. Commun.*, 1993, 687.

4 E. Aharon, A. Albo, M. Kalina and G. Frey, *Adv. Funct. Mater.*, 2006, **16**, 980.

5 (*a*) L. H. Xie, C. R. Yin, W. Y. Lai, Q. L. Fan and W. Huang, *Prog. Polym. Sci.*, 2012, **37**, 1192; (*b*) S. Kappaun, C. Slugovc and E. J. W. List, *Adv. Polym. Sci.*, 2008, **212**, 273; (*c*) A. Monkman, C. Rothe, S. King and F. Dias, *Adv. Polym. Sci.*, 2008, **212**, 187; (*d*) S. A. Chen, H. H. Lu and C. W. Huang, *Adv. Polym. Sci.*, 2008, **212**, 49.

6 (*a*) N. Bitinis, M. Hernandez, R. Verdejo, J. M. Kenny and M. A. Lopez-Manchado, *Adv. Mater.*, 2011, **23**, 5229; (*b*) M. Ogawa and K. Kuroda, *Chem. Rev.*, 1995, **95**, 399; (*c*) F. López Arbeloa, V. Martínez Martínez, T. Arbeloa and I. López Arbeloa, *J. Photochem. Photobiol., C*, 2007, **8**, 85; (*d*) G. Leone, A. Boglia, F. Bertini, M. Canetti and G. Ricci, *J. Polym. Sci., Part A: Polym. Chem.*, 2010, **48**, 4473.

7 (*a*) E. Ruiz-Hitzky, P. Aranda, M. Darder and M. Ogawa, *Chem. Soc. Rev.*, 2011, **40**, 801; (*b*) J. Pyun and K. Matyjaszewski, *Chem. Mater.*, 2001, **13**, 3436.

8 (*a*) C. J. Hawker, A. W. Bosman and E. Harth, *Chem. Rev.*, 2001, **101**, 3661; (*b*) J. Nicolas, Y. Guillaneuf, C. Lefay, D. Bertin, D. Gigmes and B. Charleux, *Prog. Polym. Sci.*, 2013, **38**, 63; (*c*) M. A. Tasdelen, J. Kreutzer and Y. Yagci, *Macromol. Chem. Phys.*, 2010, **211**, 279; (*d*) M. K. Brinks and A. Studer, *Macromol. Rapid Commun.*, 2009, **30**, 1043; (*e*) R. Barbey, L. Lavanant, D. Paripovic, N. Schüwer, C. Sugnaux, S. Tugulu and H.-A. Klok, *Chem. Rev.*, 2009, **109**, 5437; (*f*) X. Fan, C. Xia and R. C. Advincula, *Langmuir*, 2003, **19**, 4381.

9 (*a*) S.-M. Shau, T.-Y. Juang, W.-H. Ting, M.-Y. Wu, S. A. Dai and R.-J. Jeng, *Polym. Chem.*, 2011, **2**, 2341; (*b*) B. Lego, M. Francois, W. G. Skene and S. Giasson, *Langmuir*, 2009, **25**, 5313.

10 (*a*) K. Watanabe, K. Suda and K. Akagi, *J. Mater. Chem. C*, 2013, **1**, 2797; (*b*) M.-Q. Zhao, Q. Zhang, J.-Q. Huang and F. Wei, *Adv. Funct. Mater.*, 2012, **22**, 675; (*c*) S. Förster and T. Plantenberg, *Angew. Chem., Int. Ed.*, 2002, **41**, 688; (*d*) S. Cao, L. Fang, Z. Zhao, Y. Ge, S. Piletsky and A. P. F. Turner, *Adv. Funct. Mater.*, 2013, **23**, 2162.

11 (*a*) Y. Bai, J. Feng, Y. F. Liu, J. F. Song, J. Simonen, Y. Jin, Q. D. Chen, J. Zi and H. B. Sun, *Org. Electron.*, 2011, **12**, 1927; (*b*) W. H. Koo, S. M. Jeong, F. Araoka, K. Ishikawa, S. Nishimura, T. Toyooka and H. Takezoe, *Nat. Photonics*, 2010, **4**, 222; (*c*) T. Bocksrocker, J. Hoffmann, C. Eschenbaum, A. Pargner, J. Preinfalk, F. Maier-Flaig and U. Lemmer, *Org. Electron.*, 2013, **14**, 396.

12 (*a*) P. Escalé, L. Rubatat, L. Billon and M. Save, *Eur. Polym. J.*, 2012, **48**, 1001; (*b*) M. Hernandez-Guerrero and M. H. Stenzel, *Polym. Chem.*, 2012, **3**, 563.

13 J. Ding, M. Day, G. Robertson and J. Roovers, *Macromolecules*, 2002, **35**, 3474.

14 G. Leone, U. Giovanella, F. Bertini, W. Porzio, F. Meinardi, C. Botta and G. Ricci, *J. Mater. Chem. C*, 2013, **1**, 1450.

15 V. S. Smitha, K. A. Manjumol, S. Ghosh, M. Brahmakumar, C. Pavithran, P. Perumal and K. G. Warrier, *J. Am. Ceram. Soc.*, 2011, **94**, 1731.

16 J. Moreau, U. Giovanella, J.-P. Bombenger, W. Porzio, V. Vohra, L. Spadacini, G. Di Silvestro, L. Barba,

G. Arrighetti, S. Destri, M. Pasini, M. Saba, F. Quochi, A. Mura, G. Bongiovanni, M. Fiorini, M. Uslenghi and C. Botta, *ChemPhysChem*, 2009, **10**, 647.

17 (*a*) S. M. Auerbach, K. A. Carrado and S. M. Dutta, *Handbook of Layered Materials*, Marcel Dekker Inc., New York, 2004; (*b*) L. A. Utracki, B. Broughton, N. González-Rojano, L. Hecker de Carvalho and C. A. Achete, *Polym. Eng. Sci.*, 2011, 569.

18 (*a*) L. Tebben and A. Studer, *Angew. Chem., Int. Ed.*, 2011, **50**, 5034; (*b*) U. Velten, R. A. Shelden, W. R. Caseri and U. W. Suter, *Macromolecules*, 1999, **32**, 3590.

19 H. Hata, Y. Kobayashi and T. Mallouk, *Chem. Mater.*, 2007, **19**, 79.

20 (*a*) U. Giovanella, G. Leone, G. Ricci, T. Virgili, I. Suarez Lopez, S. K. Rajendran and C. Botta, *Phys. Chem. Chem. Phys.*, 2012, **14**, 13646; (*b*) J. Bujdak, N. Iyi, Y. Kaneko, A. Czímerová and R. Sasai, *Phys. Chem. Chem. Phys.*, 2003, **5**, 4680; (*c*) J. Bujdák and N. Iyi, *Colloid Polym. Sci.*, 2009, **287**, 157.

21 J. R. Tozoni, F. E. G. Guimarães, T. D. Z. Atvars, B. Nowacki, A. Marlleta, L. Akcelrud and T. J. Bonagamba, *Eur. Polym. J.*, 2011, **47**, 2259.

22 (*a*) H. H. Fan, L. Guo, K. F. Li, M. S. Wong and K. W. Cheah, *J. Am. Chem. Soc.*, 2012, **134**, 7297; (*b*) P. L. Wu, P. F. Xia, Z. H. Li, X. J. Feng, H. L. Tam, K. F. Li, Y. Jiao, M. S. Wong and K. W. Cheah, *Chem. Commun.*, 2009, 5421.

23 W. C. Tsoi, A. Charas, A. J. Calby, G. Khalil, A. M. Adawi, A. Iraqi, B. Hunt, J. Morgado and D. G. Lidzey, *Adv. Funct. Mater.*, 2008, **18**, 600.

24 F. Jaramillo-Isazaab and M. L. Turner, *J. Mater. Chem.*, 2006, **16**, 83.

25 Y. Zou, J. Zou, T. Ye, C. Yang, H. Wu, D. Ma, J. Qin and Y. Cao, *Adv. Funct. Mater.*, 2013, **23**, 1781.

26 (*a*) F. Galeotti, V. Calabrese, M. Cavazzini, S. Quici, C. Poleunis, S. Yunus and A. Bolognesi, *Chem. Mater.*, 2010, **22**, 2764; (*b*) M. Srinivasarao, D. Collings, A. Philips and S. Patel, *Science*, 2001, **292**, 79; (*c*) H. Yabu and M. Shimomura, *Chem. Mater.*, 2005, **17**, 5231.

27 Fluorescence microscopy images were taken with three different excitation filters. UV: 356 nm excitation bandpass and 420 nm filter cut. Blue: 470 nm bandpass and 515 nm filter cut. Green: 353 nm bandpass and 515 nm filter cut.

28 (*a*) L. A. Connal and G. G. Qiao, *Adv. Mater.*, 2006, **18**, 3024; (*b*) L. A. Connal and G. G. Qiao, *Soft Matter*, 2007, **3**, 837.

29 G. Leone, U. Giovanella, W. Porzio, C. Botta and G. Ricci, *J. Mater. Chem.*, 2011, **21**, 12901.

30 (*a*) B. P. Nair and C. Pavithran, *Langmuir*, 2010, **26**, 12948; (*b*) X. Xu, L. P. Heng, X. J. Zhao, J. Ma, L. Lin and L. Jiang, *J. Mater. Chem.*, 2012, **22**, 10883.

31 J. C. Hsu, K. Sugiyama, Y. C. Chiu, A. Hirao and W. C. Chen, *Macromolecules*, 2010, **43**, 7151.

32 G. Widawski, M. Rawiso and B. Francois, *Nature*, 1994, **369**, 387.